



The determination of variogram in the presence of horizontal wells - An application to a conglomerate reservoir modeling, East China



Yuming Liu^{a,b,c}, Bo Zhang^{c,*}, Yue Dong^d, Zhipeng Qu^e, Jiagen Hou^b

^a China University of Petroleum - Beijing, State Key Laboratory of Petroleum Resources and Prospecting, China

^b China University of Petroleum - Beijing, College of Geosciences, China

^c The University of Alabama, The Department of Geological Sciences, USA

^d China University of Geosciences, School of Energy Resources, China

^e Geophysical Research Institute of Shengli Oilfield, SINOPEC, China

ARTICLE INFO

Keywords:

Variogram
Reservoir modeling
Horizontal wells
Conglomerate reservoirs

ABSTRACT

Building a reliable numerical geological model is critical in reservoir development and management. Inferring a stable 3D variogram is one of the most important processes in the building of numerical geological model. We usually can obtain a well-defined vertical variogram from wells in most cases due to the regular sampling in the vertical direction. The quality of horizontal variogram highly depends on the number of wells, geometric of the well locations, and the trajectory of wells. Horizontal wells usually have preferred trajectory directions due to the geological and geomechanical consideration. As a result, it is very difficult to obtain a reliable horizontal variogram by using the data of horizontal wells. We proposed a three-step procedure to infer the horizontal variogram by integrating geological, seismic, and horizontal well data. We first use the geological information and P-impedance to infer the approximate major azimuth of horizontal variogram. We then obtain the range of the variogram for each horizontal well using the data of horizontal section. We finally determine the major, minor direction and corresponding ranges by least-square fitting the ranges computed using each horizontal well. We illustrate our workflow by applying it to a conglomeratic reservoir modeling, East China. The modeled reservoir properties have a very good correlation with the production data.

1. Introduction

Establishing a stable 3D variogram function is vital for the geostatistical reservoir modeling (Gringarten and Deutsch, 2001). The variogram function statically describes the spatial variability and continuity of a reservoir property such as lithofacies, porosity or permeability (Dubrule, 1998; Gringarten, 1999). The semivariogram for lag distance h is defined as half the average squared differences of values separated approximately by h (Matheron, 1963; Cressie, 1991; Chambers et al., 2000). We usually employ experimental variogram to describe the spatial continuity of the data considering the limited or unregulated distribution of samples. In the real application, we need to replace the experimental variogram with an acceptable variogram model for kriging or stochastic simulation of the reservoir properties (Olea, 1995; Coburn, 2012). The variogram model is a function fitted by a measure of variability between pairs of points at various distances. The commonly used variogram models include spherical, exponential,

Gaussian, and power functions (Deutsch and Journel, 1998; Pyrcz and Deutsch, 2014). The reservoir properties usually illustrate anisotropic features due to the spatial heterogeneity introduced by geological factors such as paleogeomorphology (Lassiter et al., 1986; Li et al., 2018; Liu et al., 2018a; Wang et al., 2018). As a result, we need to employ an anisotropic ellipse to describe the 2D horizontal continuity of the reservoir properties (Shepherd, 2009). The most challenge tasks of obtaining the anisotropic ellipse are determining the major, and minor directions of the ellipse and corresponding ranges of the axis of the ellipse. There are two main steps in determining the parameters of the anisotropic ellipse (Larrondo et al., 2003; Rezvandehy and Deutsch, 2018). The first step is obtain the parameters of the variogram model along user-defined directions. The second step is obtaining the parameters of ellipse by fitting the ranges of the variogram model obtained in the first step.

We need an even distribution and sufficient number of samples to obtain a reliable variogram model (Bohling, 2005; Liu et al., 2018b; Xu

* Corresponding author. The University of Alabama, The Department of Geological Sciences, 2003 Bevell Building, 201 7th Ave, Tuscaloosa, AL, 35487, USA.
E-mail addresses: liuym@cup.edu.cn (Y. Liu), bzhang33@ua.edu (B. Zhang), cugb_dongyue@hotmail.com (Y. Dong), 16071152@qq.com (Z. Qu), houjg63@cup.edu.cn (J. Hou).

<https://doi.org/10.1016/j.petrol.2018.10.034>

Received 20 May 2018; Received in revised form 19 September 2018; Accepted 11 October 2018

Available online 15 October 2018

0920-4105/ © 2018 Elsevier B.V. All rights reserved.

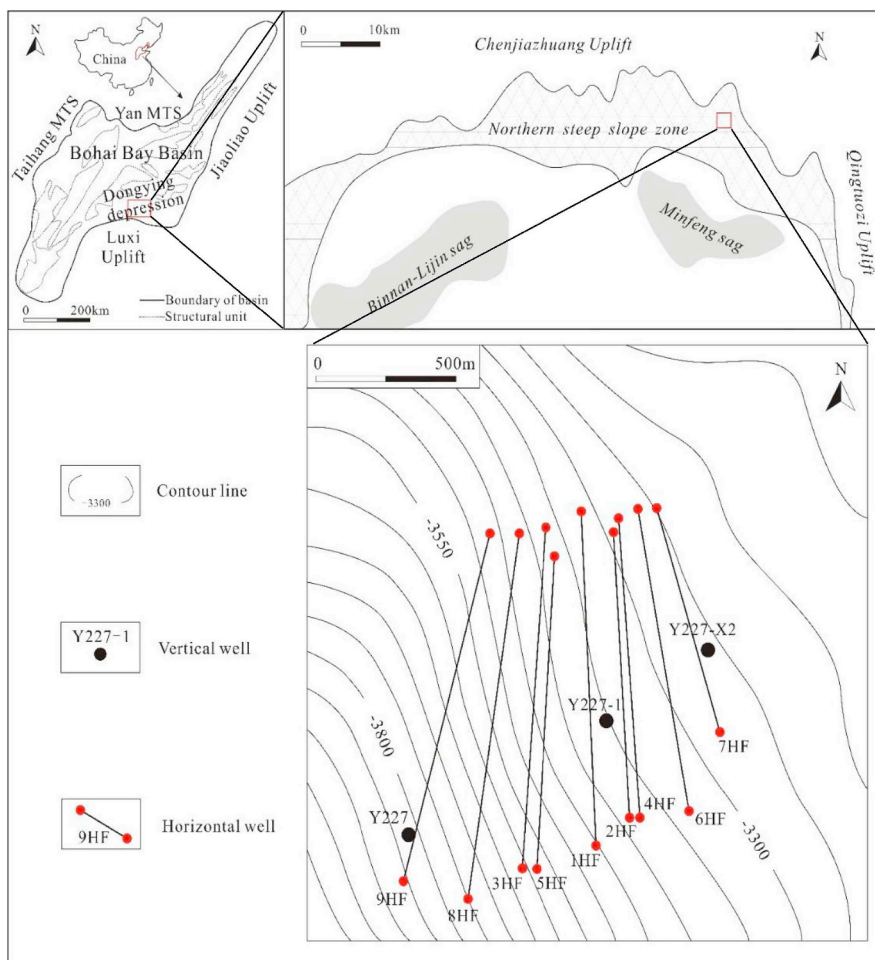


Fig. 1. Locations of studied area.

Table 1
Typical Chronostratigraphy of the north Dongying depression (modified from Sun, 2003 and Liu et al., 2017).

Chronological Era	Stratigraphy Period	Lithostratigraphic unit Formation	Member	Structural Evolution	Thickness (m)	Lithofacies
Cenozoic	Quaternary	Pingyuan	/	Thermal subsidence	300–380	Unconsolidated sand and mud
	Neogene	Minghuazhen	/		640–700	Variegated mudstone Siltstone Sandy mudstone
		Guantao	/		250–350	Upper: celadon siltstone with brown mudstone Middle; brown, purple, celadon mudstone with silty sandstone Lower: gray gravelly sandstone, with brown and celadon mudstone, thin-bedded calcareous sandstone
	Paleogene	Dongying	/	Contraction phase	< 200	Amaranth mudstone with fine-medium sandstone, and conglomerate at the bottom
		Shahejie	S1	Deep subsiding phase	< 200	Siltstone, muddy siltstone, fine sandstone
			S2		100–200	Siltstone, muddy siltstone, fine sandstone
			S3		> 650	Dark mudstone
		S4	Expansion rifting phase	600–1000	Conglomerate, pebbly sandstone, mudstone	
		Kongdian	/	Initial rifting phase	< 100	Gravelly sandstone, with mudstone and muddy sandstone Amaranth mudstone with fine-medium sandstone, and conglomerate at the bottom

et al., 2018). However, we usually have an uneven distribution of borehole locations due to the consideration of reservoir management. Nowadays, directional and horizontal drilling are the common methods used to increase production of conventional and unconventional reservoirs. We usually have limited number of horizontal wells due to the high drilling cost of horizontal wells within the reservoirs. Moreover,

the trajectory of directional and horizontal wells usually clusters in certain azimuth zone due to the geological and geomechanical consideration. As a result, it is very difficult to obtain a reliable estimation of the parameters of the variogram model by using the conventional two-step of horizontal variogram analysis. Consequently, it is hard to determine the parameters of the 2D horizontal anisotropic ellipse which



Fig. 2. Core photographs of different rock types in studied area.

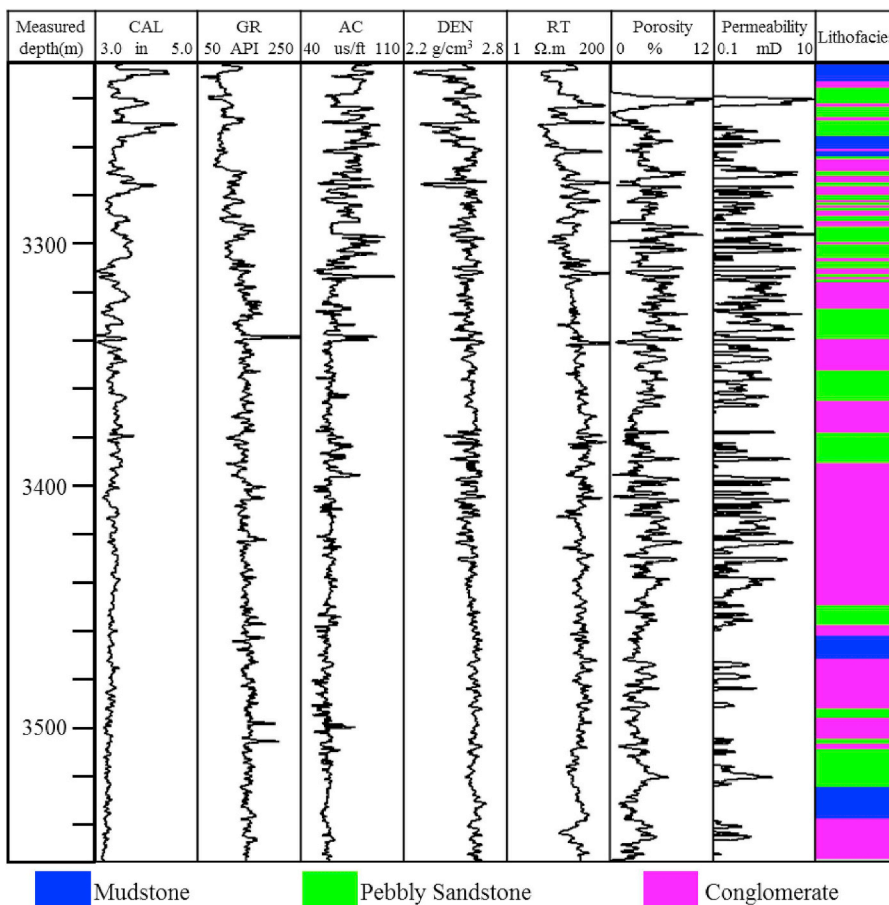


Fig. 3. A representative well with well logs.

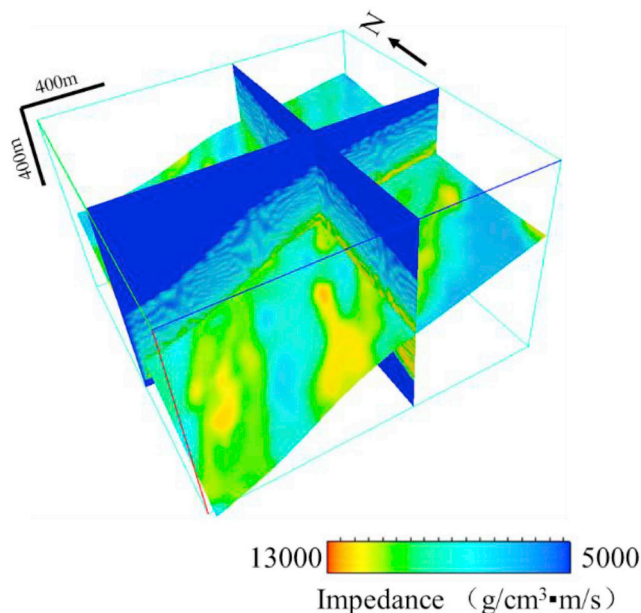


Fig. 4. 3D P-impedance volume used to determine the approximate major direction of the horizontal anisotropy model.

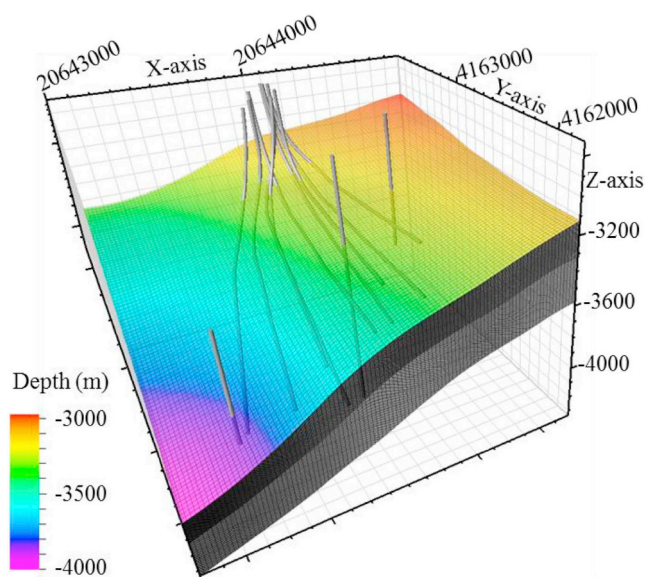


Fig. 5. 3D grid (the gray cells) of the reservoir model and the horizon used as the top boundary of the reservoir model.

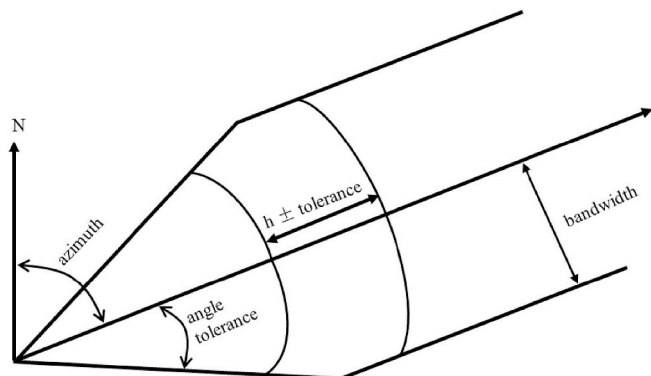


Fig. 6. The cartoon illustrating the parameters needed for variogram function computation (modified from Bohling, 2005).

are the key inputs for the following kriging or stochastic simulation of the reservoir properties.

In this paper, we proposed a three-step workflow to obtain the 2D horizontal anisotropic ellipse in the presence of horizontal wells. We assume that the paleogeomorphology of the basin determines the heterogeneity distribution of the lithofacies. We first determine the approximate major direction of the horizontal anisotropic ellipse using the paleogeomorphology of the basin. We further use the P-impedance inverted from seismic data to statistically determine the approximate azimuth zone of the major direction of the anisotropic ellipse. We then estimate parameters of variogram function for each horizontal well. The trajectory of the horizontal section of each horizontal well determines the azimuth of estimated variogram function. We finally obtain the 2D horizontal anisotropic ellipse by fitting the ranges of the variogram function of each well obtained in the second step. The major, minor and vertical directions and corresponding ranges of 3D anisotropic ellipsoid are the inputs for the following reservoir properties simulation. We illustrated our workflow by applying it to a conglomeratic reservoir modeling, East China.

2. Geological backgrounds

The Yan 227 Oilfield is located within the northern steep slope zone of Dongying Depression, Bohai Bay Basin, East China and covers an approximate area of 4 km² (Fig. 1). The Bohai Bay Basin is a rift basin and the Dongying Depression is a part of the rift basin formed during the Mesozoic and Cenozoic period (Wang et al., 2017; Zhang et al., 2004). The strike and dip of the northern steep slope zone of Dongying Depression are east-west and towards to south, respectively. The target reservoir zone is within the fourth member (S4) of the Shahejie formation (Table 1). The structure of S4 member within the studied area can be characterized as a monocline with a thickness ranging from 600 to 1000 m. There is no interpreted fault for the S4 member located within our studied area. The top topography of S4 member illustrates high elevation at the northeast zone and low elevation at the southwest zone (Fig. 1). The dipping angle of the S4 member ranges from 10° to 16°. The depth of reservoir formation is approximate 3000 m at the northeast zone and 4000 m at southwest zone. The thickness of the reservoir formation is approximate 400 m. The lithofacies of the S4 member include conglomerate, pebbly sandstone, and mudstone (Fig. 2). The conglomerate is the dominated lithofacies within S4 member and the porosity is usually smaller than 4%. The porosity of the pebbly sandstone ranges from 4% to 12% and functions as the main reservoir. The black mudstone has horizontal bedding and massive bedding structure (Fig. 2) and is not the reservoir rock. The estimated geological reserve is approximate 400 × 10⁴t. Planning horizontal wells is critical to locate the pebbly sandstone and we have our first production well in September 2013.

3. Geostatistical modeling in the presence of horizontal wells

Reservoir modeling is the final step in the reservoir characterization process. Geostatistical reservoir modeling simulate the numerous solutions that satisfy the constraints imposed by the geological, seismic, petrophysics, and production data. Reservoir modeling includes four main steps: (1) data preparation and formatting, (2) 3D structural and stratigraphic modeling, (3) facies and petrophysical modeling, and (4) dynamic modeling. This paper aims developing a new workflow to estimate the variogram in the presence of horizontal wells which is the key process in the third step. The final step of the reservoir modeling is beyond the scope of this paper.

3.1. Data preparation and formatting

We have 9 horizontal and 3 vertical wells within the studied area (Fig. 1). The sampling interval of well logs is 0.125 m both for

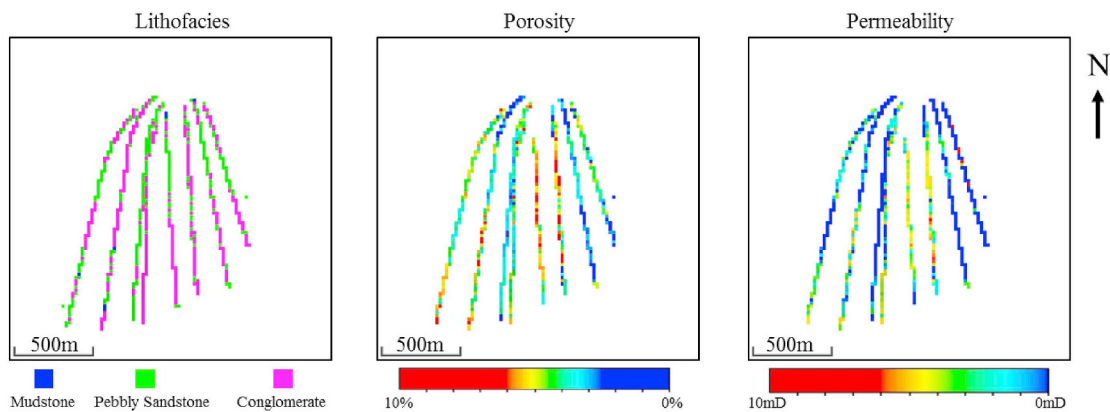


Fig. 7. The upscaled lithofacies, porosity, and permeability of horizontal wells.

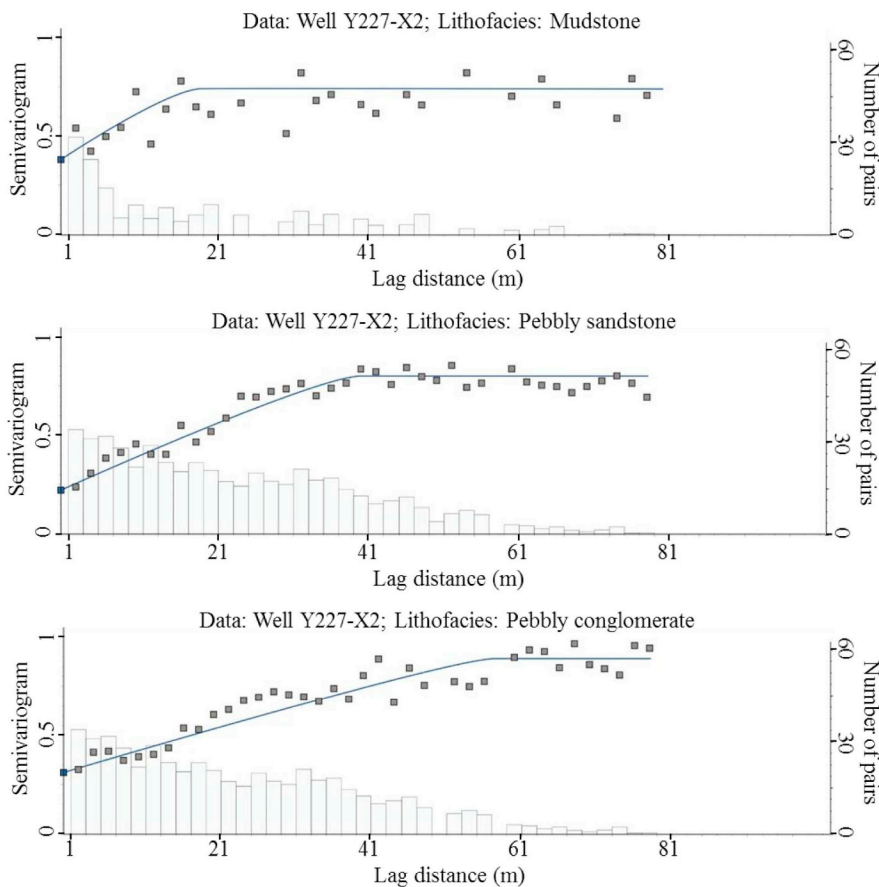


Fig. 8. The vertical variogram function of lithofacies using data of well Y227-X2.

horizontal and vertical wells. Both horizontal and vertical wells have caliper (CNL), gamma ray (GR), sonic (AC), density (DEN), and resistivity (RT) logs (Fig. 3). Fig. 3 also show the interpreted porosity, permeability and lithofacies logs from the oil company. The geologists from the oil company did not further interpret the beds within the S4 member considering the complex lithofacies within S4 member. As a result, we only have one zone in our reservoir model. We select well Y227-1 as the blind well to validate the simulated models.

We also have 3D acoustic impedance volume from the oil company inverted from poststack seismic data (Fig. 4). The geophysicists from the oil company already converted 3D acoustic impedance from time domain to depth domain. The sample interval of the acoustic

impedance is 12 m.

3.2. 3D structural and stratigraphic modeling

We employ two interpreted horizons provided by the oil company as the upper and lower boundaries for building our reservoir model. There is no interpreted faults in our reservoir modeling. The depth of the upper boundary is approximate 3100 m at the northeast corner and 4000 m at the southwest corner, respectively (Fig. 5). The width and length of our model are 2000m and 2000m, respectively. The height of our model is 400 m approximately. The width and length of cell are 20 m and 20 m, respectively. The height of cell is approximate 2 m. The

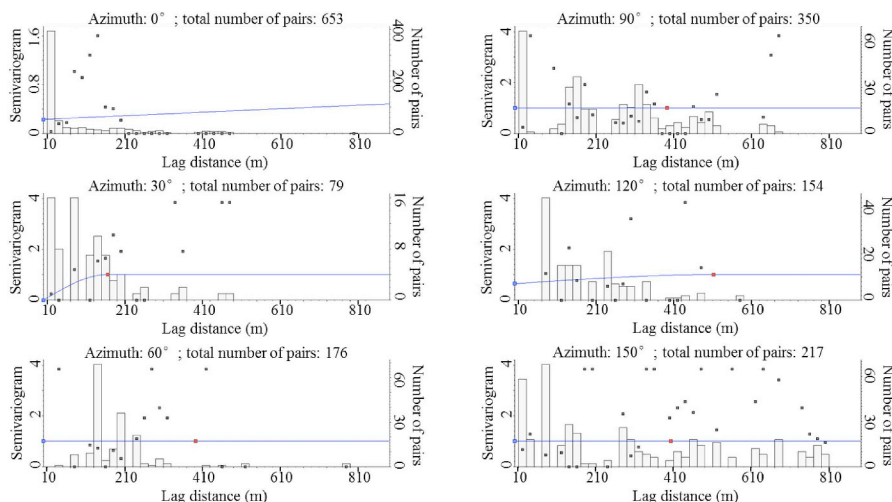


Fig. 9. The horizontal variogram analysis of lithofacies using the conventional method along six different azimuths.

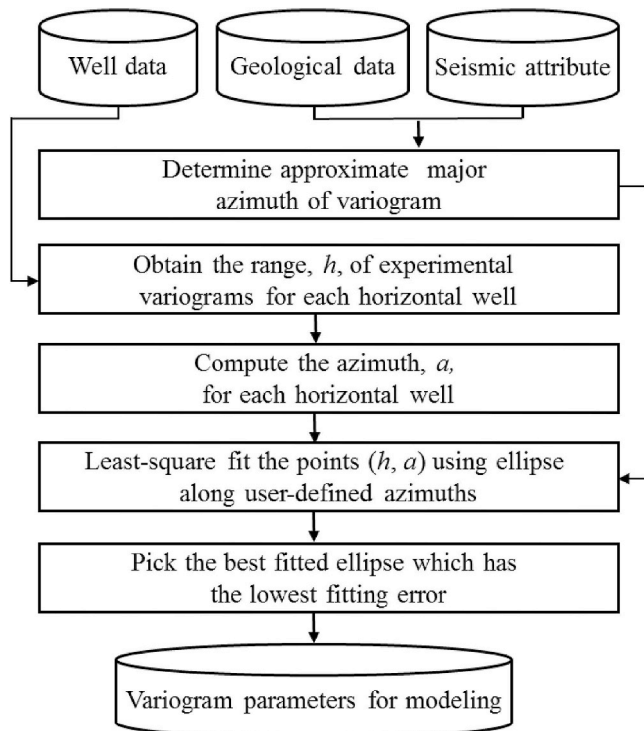


Fig. 10. The workflow for the horizontal anisotropy model.

total cell number is 2,000,000 (100 × 100 × 200). Fig. 5 illustrates the 3D grid used to define our reservoir model.

3.3. The determination of 3D variogram for lithofacies and petrophysical modeling

Variogram has become the central tool for geostatistics analysis.

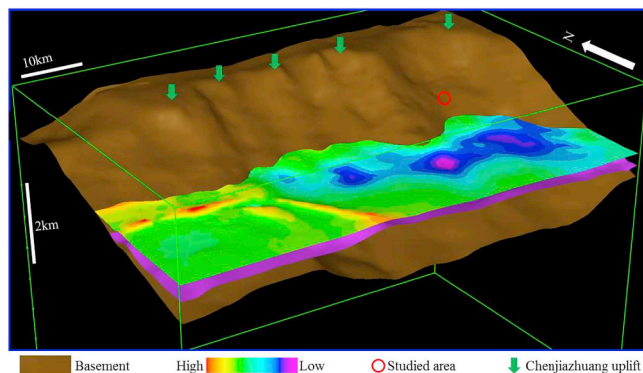


Fig. 11. The 3D paleogeomorphology before the deposition of S4 member within our basin.

Semivariogram $\gamma(\mathbf{h})$ characterizes the spatial continuity or roughness of a data set Z (Matheron, 1965).

$$\gamma(\mathbf{h}) = \frac{1}{2} \text{var} [Z(\mathbf{x}) - Z(\mathbf{x} + \mathbf{h})] = \frac{1}{2} E \{ [Z(\mathbf{x}) - Z(\mathbf{x} + \mathbf{h})]^2 \} \quad (1)$$

where $Z(\mathbf{x})$ and $Z(\mathbf{x} + \mathbf{h})$ are the values of Z at places \mathbf{x} and $\mathbf{x} + \mathbf{h}$, and E denotes the expectation. The semivariogram depends only on \mathbf{h} . The semivariogram defined in equation (1) is a theoretical function. Experimental semivariogram $\hat{\gamma}(\mathbf{h})$ is the actual realization of semivariogram on the ground and one that we estimated from data, $z(\mathbf{x}_j)$

$$\hat{\gamma}(\mathbf{h}) = \frac{1}{2m(\mathbf{h})} \sum_{j=1}^{m(\mathbf{h})} \{z(\mathbf{x}_j) - z(\mathbf{x}_j + \mathbf{h})\}^2 \quad (2)$$

where $m(\mathbf{h})$ is the number of paired comparisons at lag \mathbf{h} . By incrementing \mathbf{h} in steps we obtain an ordered set of values. We obtain the experimental variogram by mathematical fitting the ordered set of values.

The reservoir usually shows different autocorrelation structures in different directions and the phenomenon is called geometric

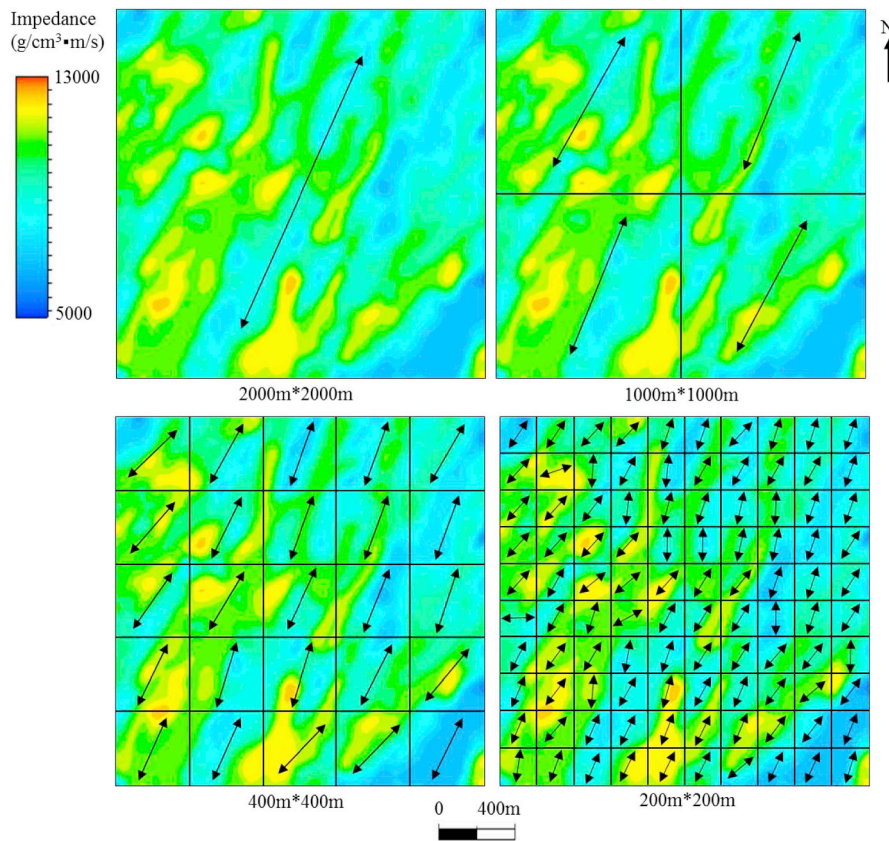


Fig. 12. The local varying anisotropy analysis of the averaged P-impedance using difference window sizes.

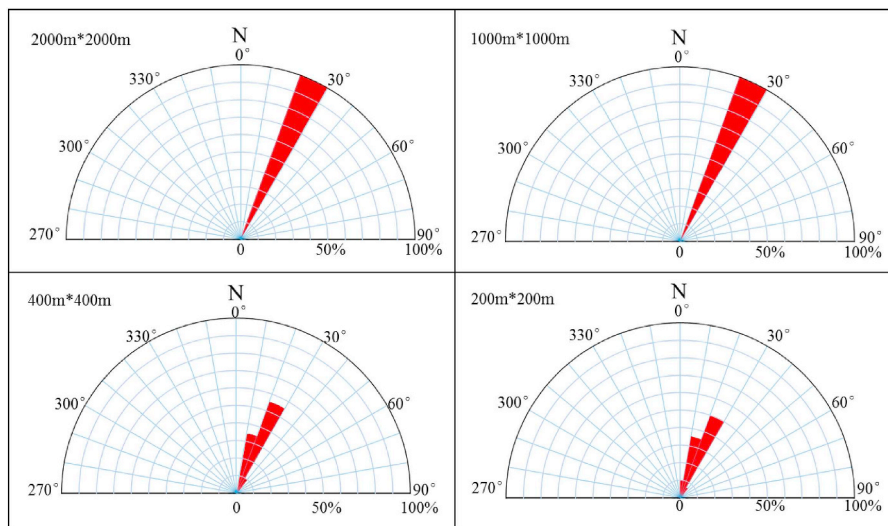


Fig. 13. The rose diagram of the azimuth of the LVA.

anisotropy. We need to define the three principal, orthogonal directions to describe the geometric anisotropy. There are two steps in obtaining the three principal direction. The first step is computing semivariance values for data pairs falling within certain directional bands as well as

falling within the prescribed lag limits. The directional bands are specified by a given azimuthal direction, angular tolerance, and bandwidth (Bohling, 2005. Fig. 6). The second step is fitting the lags of semivariance using an ellipse function. The azimuth of the long and short axes

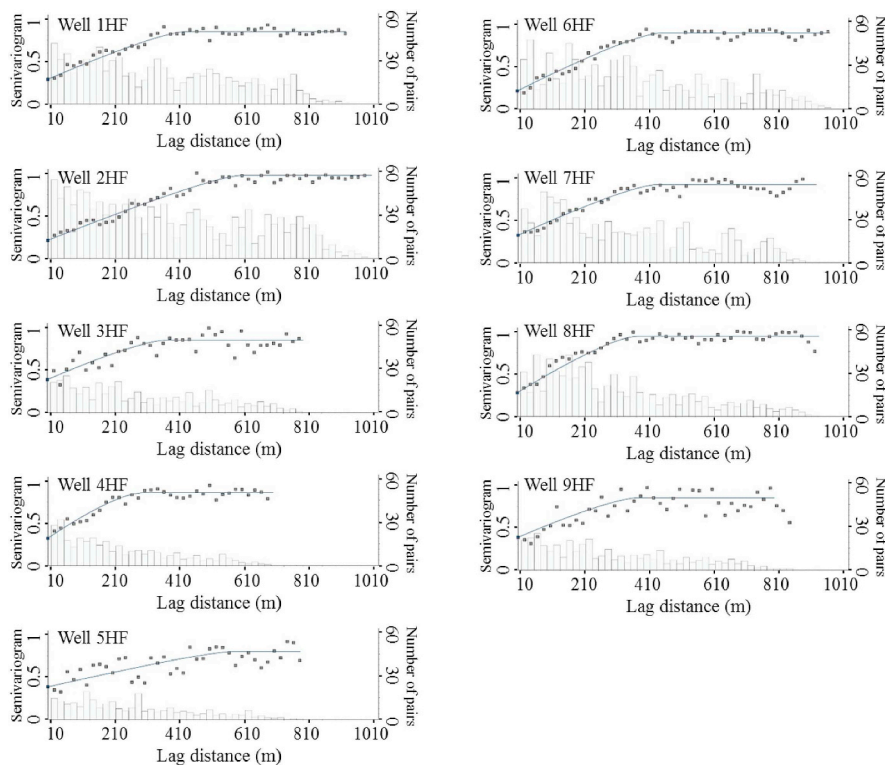


Fig. 14. The variogram analysis of lithofacies using nine horizontal wells.

Table 2
The computed variogram function parameters for each horizontal well.

Well	Horizontal Section Azimuth (°)	Length of Horizontal Section (m)	Type of variogram	Range (m)		
				Mudstone	Pebbly sandstone	Conglomerate
1HF	174.5	890	Spherical	581.7	431.1	766.5
2HF	176.1	920	Spherical	552.6	447.0	649.8
3HF	185.3	1010	Spherical	514.8	599.1	762.9
4HF	176.2	980	Spherical	199.2	431.1	564.3
5HF	180.8	1020	Spherical	564.3	376.8	607.8
6HF	169.1	995	Spherical	519.0	376.8	519.0
7HF	163.4	805	Spherical	521.1	304.8	616.8
8HF	188.9	1000	Spherical	647.1	431.7	693.6
9HF	192.3	1010	Spherical	629.7	575	796.8

of the ellipse function is regards as the major and minor directions.

We follow the general workflow proposed by the Schlumberger software Petrel for variogram analysis (Schlumberger, 2014). There are three main steps in the variogram analysis for 3D modeling: (1) petrophysical properties upscaling, (2) vertical variogram analysis, and (3) horizontal variogram analysis.

Fig. 7 shows the upscaled lithofacies, porosity, and permeability properties respectively. We use the vertical well to obtain the vertical variogram function. Fig. 8 shows the results of variogram analysis using vertical well. Fig. 9 shows the results of horizontal variogram analysis

for pebbly sandstone along six different azimuths. The minimum and maximum lag distance 10 m and 810 m. The lag increment, search radius, bandwidth, and tolerance angle for the variogram analysis are 20 m, 800 m, 50 m and 15°, respectively. The histogram in Fig. 9 show the number of sample pair within each lag zone. The squares in Fig. 9 are the average variogram within each lag zone and are the input for variogram function fitting. The blue curves are the fitted spherical variogram function. The left and right vertical axes of Fig. 9 are the variogram and number of sample pairs within each lag zone. Note that the averaged variogram samples irregularly deviate from the fitted

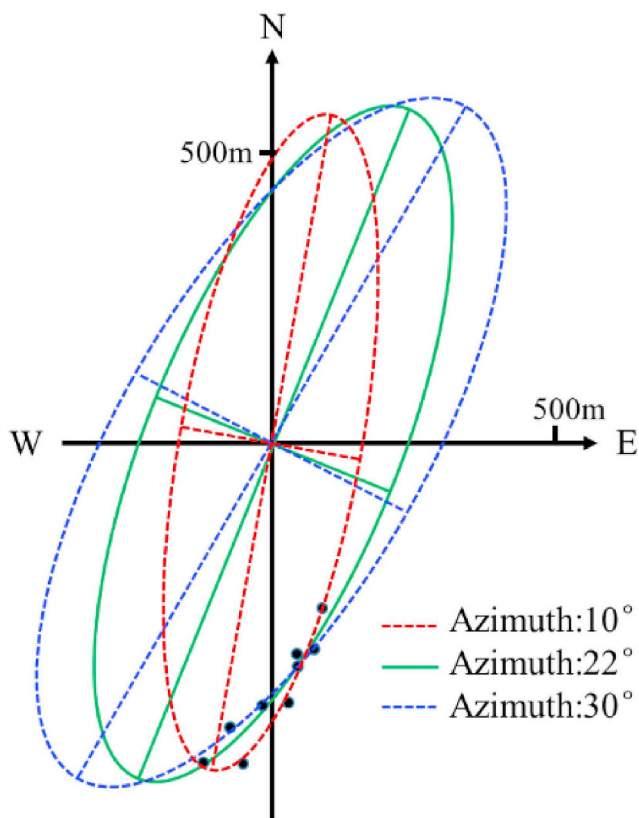


Fig. 15. The cartoon illustrating the determination of the major direction of the horizontal anisotropy ellipse.

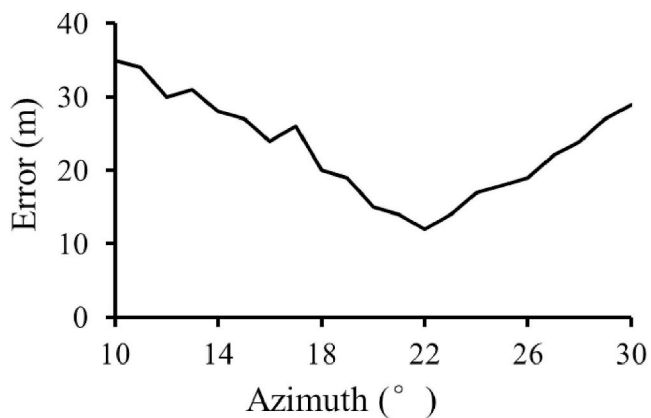


Fig. 16. The error between the fitted ellipse and samples varying with azimuth.

variogram function and this phenomena indicates the low quality of variogram analysis.

In this paper, we propose a three-step workflow to obtain the horizontal variogram function (Fig. 10). We first determine the approximate major azimuth of the horizontal variogram by integrating geological information and seismic attribute analysis. We then obtain the

Table 3
The parameters of the horizontal anisotropic ellipse for lithofacies.

Lithofacies	Horizontal variogram parameters			
	Major direction azimuth	Major range	Minor range	Vertical range
	(°)	(m)	(m)	(m)
Mudstone	20	630	384	19
Pebbly sandstone	22	641	224	40
Conglomerate	24	746	458	57

range, h , of the variogram function and compute the azimuth, a , of trajectory for each horizontal well. The third step starts with least-square fitting the points (h, a) using ellipse along user-defined azimuths. The zone of user-defined azimuth centers at the approximate major azimuth obtained in the first step and increase at a step of 1° . We finally pick the best fitted ellipse which has the lowest fitting error. We use the following the equation to estimate the fitting error

$$error = \frac{1}{N} \sum_{i=1}^N |h_i - h'_i| \tag{3}$$

where N is the total number of horizontal wells, h_i is the fitted range along the trajectory azimuth of the i^{th} well, h'_i is the range obtained in the second step of our workflow.

3.3.1. Determine the approximate major direction of horizontal variogram

The paleogeomorphology determines both the sediment transport direction and the distribution of lithofacies (Deng et al., 2001). As a result, the horizontal variogram function should have the longest range along direction of sediment transport. The S4 member within the Dongying Depression was deposited at the rifting stage of Bohai Bay basin (Chang, 1991; Hu et al., 2001; Feng et al., 2013). Fig. 11 illustrates the paleogeomorphology before the deposition of S4 member interpreted from regional study from the oil company. The brown surface is the basement of our basin. The two colorful surfaces are two representative tops beneath the S4 member. The sediments of S4 member within our studied area (indicated by the red circle) came from the eroded and weathered geological materials of Chenjiazhuang uplift (indicated by the green arrow) (Kong, 2000; Zhang and Yang, 2012; Xian et al., 2014; Dong et al., 2015). The sediment sources and the paleogeomorphology together indicate that the major direction of the horizontal variogram is approximate along the azimuth of NNE.

We further valid the approximated major direction of the horizontal variogram by analysis the locally varying anisotropy (LVA) of P-impedance inverted from seismic data (Hassanpour and Deutsch, 2008). Fig. 12 shows the averaged P-impedance for our target zone. The black arrows in Fig. 12 indicate the LVA for the P-impedance. We consider four different window sizes for LVA analysis. Figures 13 show the statistical analysis for the azimuth of the LVA shown Fig. 12. Fig. 13 indicate the azimuth of the LVA ranges from 10° to 30° degree and this azimuth zone functions as the constraints for the following determination of major direction.

3.3.2. Variogram analysis for each horizontal well

We only use the data within the horizontal sections of the horizontal wells. Fig. 14 shows the variogram analysis results of pebbly sandstone

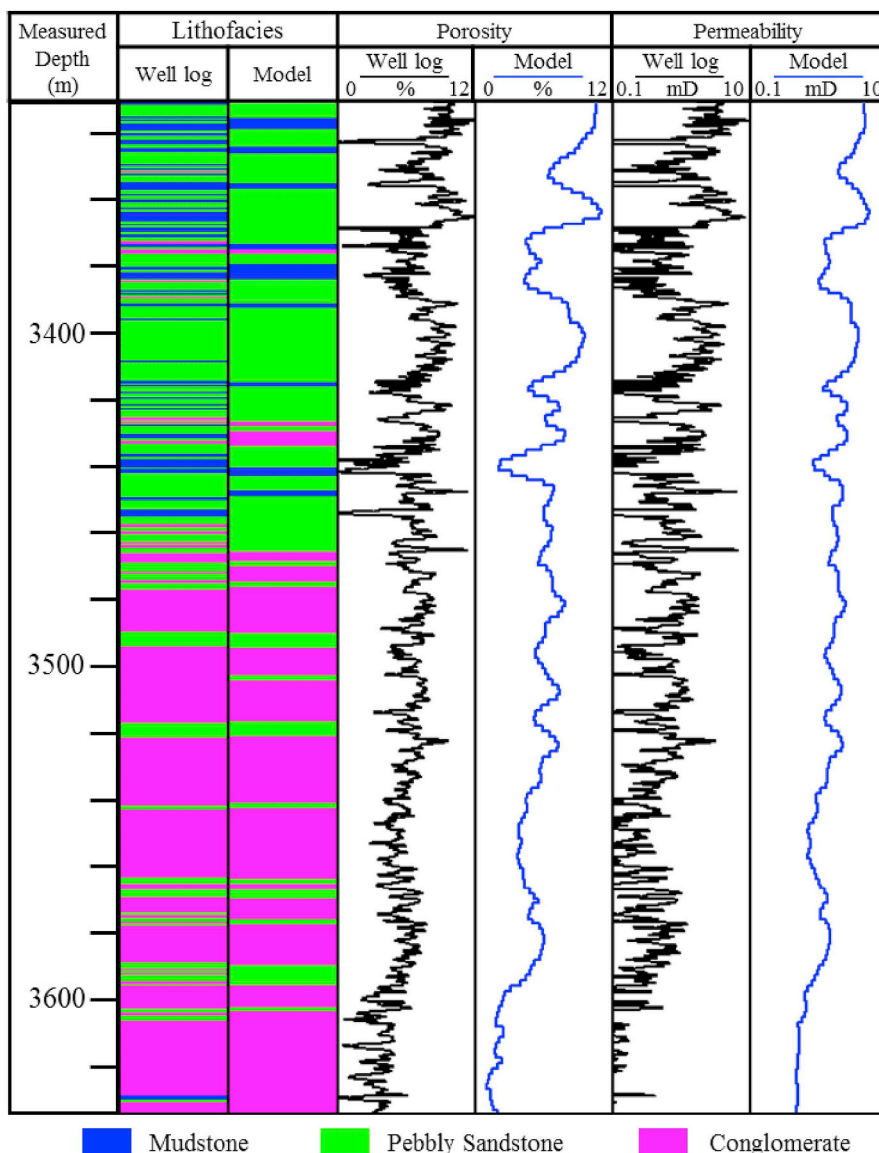


Fig. 17. The modeled reservoir properties along the trajectory of the blind well Y227-1.

for nine horizontal wells within our studied area. The minimum lag distance 10 m and the maximum lag distance equals the length of the horizontal section of each horizontal well. The lag increment is 20 m. The histogram in Fig. 14 show the number of sample pair within each lag zone. The squares in Fig. 14 are the average variogram within each lag zone and are the input for variogram function fitting. The blue curves are the fitted spherical variogram function. The left and right vertical axes of Fig. 14 are the variogram and number of sample pairs within each lag zone. Note that we now have enough point pairs for the variogram analysis for all the horizontal wells. The fitted variogram functions in Fig. 14 have an obvious visual improvement when compared to those show in Fig. 9. Table 2 shows the obtained parameters of variogram function for each horizontal well.

3.3.3. Horizontal geometric anisotropy fitting

The range and azimuth pair (h, a) of each well is the input for the geometric anisotropy determination. Fig. 15 shows representative fitted geometric anisotropy ellipses for the pebbly sandstone lithofacies using the nine range and azimuth pairs along the azimuth of 10°, 30°, and 22°, respectively. The start and end scanning azimuth is 10° and 30° according to the geological and seismic impedance analysis. The increment is 1° in our study. Fig. 16 shows the error of the fitted ellipse varying with scanning azimuth angle. Note that azimuth 22° has the least error and it is regarded as the major direction for the pebbly sandstone. Table 3 summarizes the inverted parameters of geometric anisotropy ellipses for the mudstone, pebbly sandstone, and conglomerate. We use same workflow to obtain the parameters of geometric anisotropy ellipses for the porosity and permeability properties of the

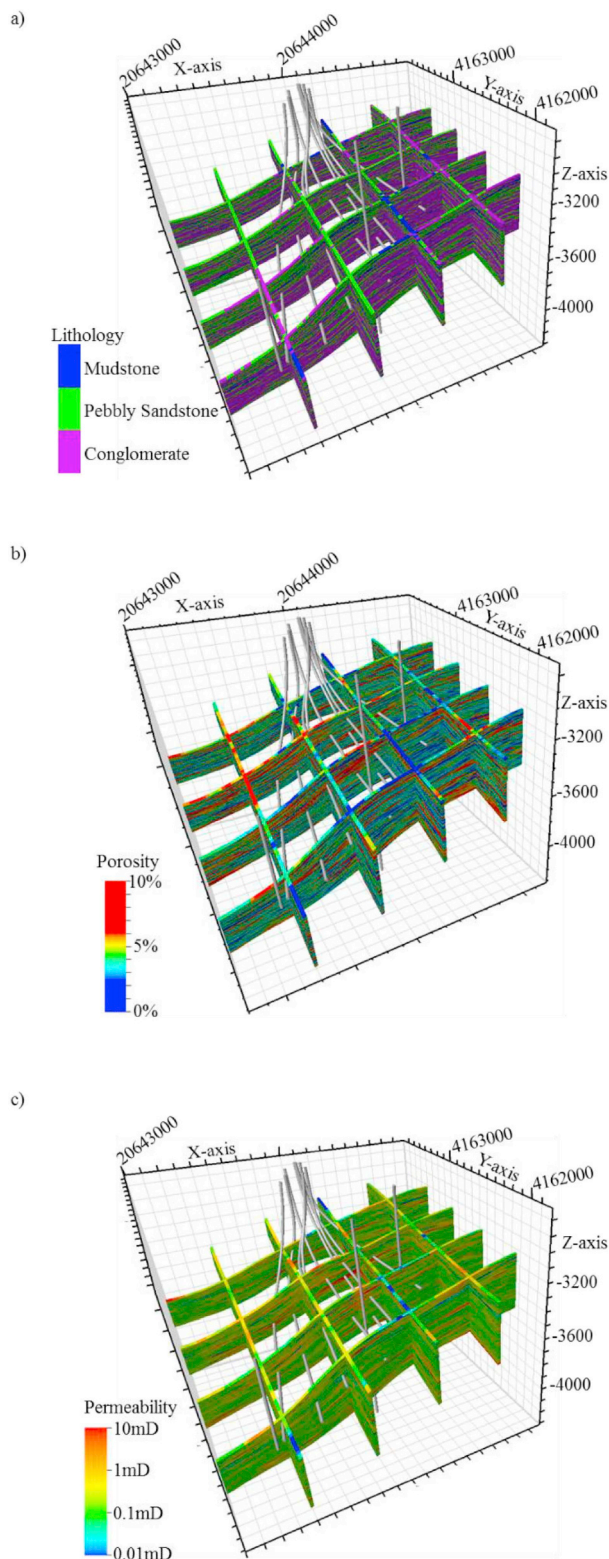


Fig. 18. The selected (a) lithofacies, (b) porosity, and (c) permeability models.

reservoir.

3.4. Numerical reservoir properties modeling results

The inputs for the reservoir properties modeling include the results of the vertical and horizontal experimental variogram, well logs, and P-impedance. The up-scaled well logs function as the hard data. Our reservoir model consists of 200 layers along the vertical direction and 100×100 cells along horizontal directions. We employ the sequential indicator co-simulation package from software Petrel to model the lithofacies. The modeled lithofacies function as the constraint for the sequential Gaussian simulation of porosity model. The modeled lithofacies and porosity model together function as the constraints for the sequential Gaussian simulation of permeability model. We have 20 realizations for the lithofacies, porosity, and permeability modeling respectively. We use the blind well Y227-1 to judge our simulations and choose the best matched model as the final results (Fig. 17). Fig. 18a, b, and 18c show the selected lithofacies, porosity, and permeability models, respectively. Fig. 19 shows averaged porosity maps. The windows size used to compute averaged porosity is 20 m and center at the trajectory of horizontal wells.

3.5. Correlation with the well production data

The numerical simulation of the modeled reservoir is beyond the scope of this paper. We validate our build models by visually comparing the simulated model properties and the production data. Table 4 shows the daily oil production of the first 10 days and total oil production of first 23 months of each horizontal well separately. Wells 3HF, 2HF, and 6HF have the highest production both for the first 10 days and first 23 months. Wells 1HF, 4HF, and 7HF have medium production both for the first 10 days and first 23 months. Wells 5HF, 8HF, and 9HF have the lowest production both for the first 10 days and first 23 months. Permeability is the main factor that determines the well production. We have a very good positive relationship between porosity and permeability in our studied area (Dong et al., 2015). Note that we have a very good match between the averaged porosity shown in Fig. 19 and well production. Fig. 19 illustrates that wells 3HF, 2HF, and 6HF penetrate the high porosity zones. Fig. 19 also illustrates Wells 5HF, 8HF, and 9HF penetrate the low porosity zones. Part of the trajectory of well 1HF penetrate the high porosity zone. Wells 4HF and 7HF locate at the margin of high porosity zones.

4. Conclusions

Obtaining a stable horizontal anisotropy model is one of the most important steps in reservoir modeling. It is very difficult to obtain a reliable horizontal anisotropy model based on the data of horizontal wells using the conventional workflow. We proposed a novel workflow to obtain the horizontal anisotropy model using the data of horizontal wells. We first determine the approximate azimuth zone of the major direction of the horizontal ellipse by integrating the paleogeomorphology of the basin and seismic attribute analysis. We then obtain the horizontal anisotropy model by fitting the variogram function of each horizontal well. The lag distance of the variogram must be smaller than the length of the horizontal section of the horizontal wells. The application of our method to a conglomerate reservoir illustrates that there is a good correlation between the simulated reservoir properties and production.

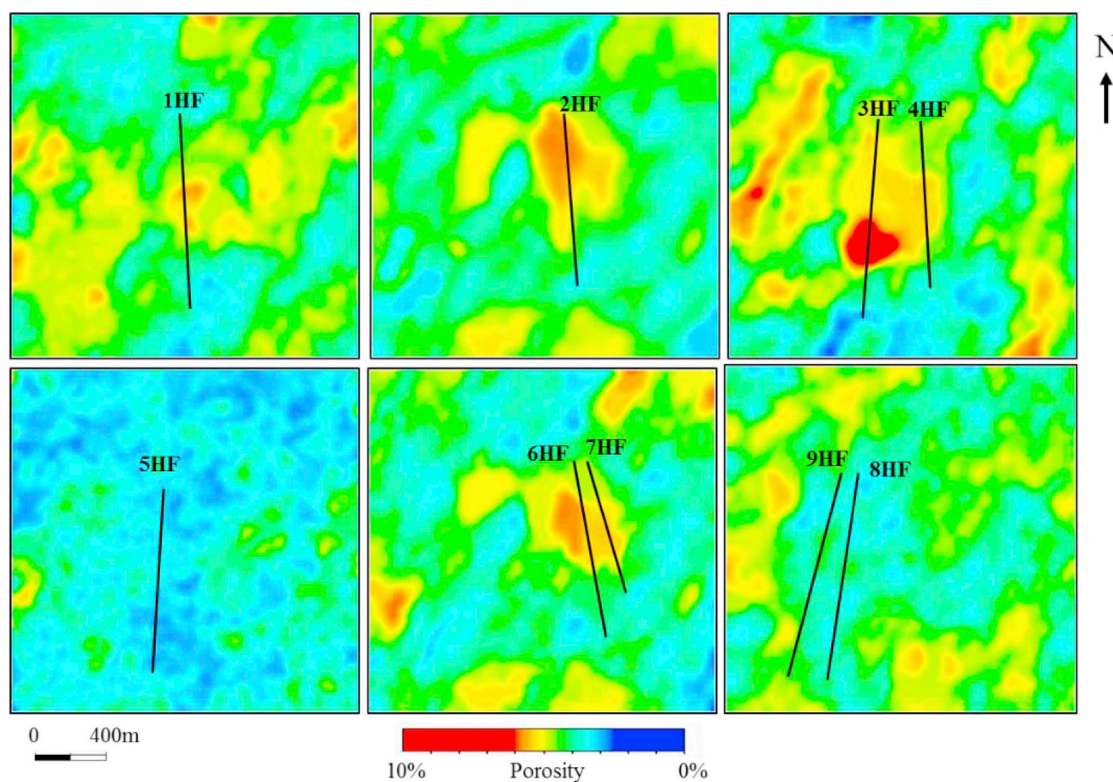


Fig. 19. The averaged porosity map.

Table 4

The Production data of each horizontal well.

Well	Production (ton)	
	Daily (First 10 days average)	Total (First 23 months)
1HF	12.6	6371
2HF	23.1	9693
3HF	31.5	13749
4HF	16.7	8002
5HF	0.2	589
6HF	21.2	8587
7HF	16.6	7743
8HF	4.5	2667
9HF	1.5	1368

Acknowledgement

The authors would like to thanks the funding support from China National Science and Technology Major Project (Grant No. 2016ZX05010-001, 2016ZX05014002-008, 2017ZX05009-001) and the National Basic Research Program of China (Grant No. 2015CB250901). The authors also thanks the SINOPEC for the data used in this study.

References

- Bohling, G., 2005. Introduction to geostatistics and variogram analysis. *Kansas geological survey* 1, 1–20.
- Chambers, R.L., Yarus, J.M., Hird, K.B., 2000. Petroleum geostatistics for non-geostatisticians: Part 1. *Lead. Edge* 19 (5), 474–479.
- Chang, C., 1991. Geological characteristics and distribution patterns of hydrocarbon deposits in Bohai Bay Basin, east China. *Mar. Petrol. Geol.* 8, 98–106.
- Coburn, T.C., 2012. Geostatistics for natural resources evaluation. *Technometrics* 42 (4), 437–438. <https://doi.org/10.1080/00401706.2000.10485733>.
- Cressie, N., 1991. *Statistics for Spatial Data*: Wiley Series in Probability and Statistics. Wiley Interscience, New York.
- Deng, H., Wang, H., Wang, D., 2001. Control of paleo-morphology to stratigraphic sequence in continental rift basins: take lower tertiary of western slope in bozhong depression as an example. *Oil Gas Geol.* 22 (4), 293–303.

- Deutsch, C.V., Journel, A.G., 1998. *GSLIB: Geostatistical Software Library and User's Guide*, second ed. Oxford Univ. Press, New York.
- Dong, Y., Hou, J., Cao, G., Liu, Y., Wang, Z., Li, J., 2015. Lithofacies and reservoir characteristics of subaqueous fan: a case from Yan 227 blok in Yanjia Oilfield. *Lithologic reservoirs* 27 (5), 60–66.
- Dubrule, O., 1998. *Geostatistics in Petroleum Geology*, vol. 38 American Association of Petroleum Geologists, Tulsa.
- Feng, Y., Li, S., Lu, Y., 2013. Sequence stratigraphy and architecture variability in late Eocene lacustrine strata of Dongying Depression, Bohai Bay Basin, eastern China. *Sediment. Geol.* 295, 1–26.
- Gringarten, E., Deutsch, C.V., 2001. Teacher's aide variogram interpretation and modeling. *Math. Geol.* 33 (4), 507–534.
- Gringarten, E., Deutsch, C.V., Jan. 1999. Methodology for variogram interpretation and modeling for improved reservoir characterization. In: *SPE Annual Technical Conference and Exhibition*. Society of Petroleum Engineers. <https://doi.org/10.2118/56654-MS>.
- Hassanpour, R.M., Deutsch, C.V., 2008. Fitting Local Anisotropy with Mass Moments of Inertia. *Center for Computational Geostatistics Annual Report*, vol. 10.
- Hu, S., O'Sullivan, P.B., Raza, A., et al., 2001. Thermal history and tectonic subsidence of the Bohai Basin, northern China: a Cenozoic rifted and local pull-apart basin. *Phys. Earth Planet. In.* 126, 221–235.
- Kong, F., 2000. Exploration technique and practice of sandy-conglomeratic fans in the northern part of Dongying depression. *Acta Pet. Sin.* 21 (5), 27–31.
- Larrondo, P.F., Neufeld, C., Deutsch, C.V., 2003. VARFIT: a Program for Semi-automatic Variogram Modelling. *CCG Annual Report 12-412*. Centre for Computational Geostatistics, University of Alberta, Edmonton, Canada.
- Lassiter, T.K., Waggoner, J.R., Lake, L.W., 1986. Reservoir heterogeneities and their influence on ultimate recovery. In: Lake, L.W., Carroll, N.B. (Eds.), *Reservoir Characterization*. Academy Press, Orlando, FL, pp. 545–560.
- Li, C., Ostadhassan, M., Guo, S., Gentzis, T., Kong, L., 2018. Application of PeakForce tapping mode of atomic force microscope to characterize nanomechanical properties of organic matter of the Bakken Shale. *Fuel* 233, 894–910.
- Liu, Y., Ma, K., Hou, J., Yan, L., Chen, F., 2018a. Diagenetic controls on the quality of the Middle Permian Lucaogou Formation tight reservoir, Southeastern Junggar Basin, Northwestern China. *J. Asian Earth Sci.*
- Liu, Y., Hou, J., Li, Y., Dong, Y., Ma, X., Wang, X., 2018b. Characterization of architectural elements of ordoevian fractured-cavernous carbonate reservoirs, Tahe Oilfield, China. *J. Geol. Soc. India* 91 (3), 315–322.
- Liu, J., Xian, B., Wang, J., Ji, Y., Lu, Z., Liu, S., 2017. Sedimentary architecture of a sub-lacustrine debris fan: eocene dongying depression, Bohai Bay basin, east China. *Sediment. Geol.* 362, 66–82.
- Matheron, G., 1963. Principles of geostatistics. *Econ. Geol.* 58 (8), 1246–1266.
- Matheron, G., 1965. *Les variables régionalisées et leur estimation*. Masson, Paris.
- Olea, R.A., 1995. Fundamentals of semivariogram estimation, modeling, and usage. In: Yarus, J.M., Chambers, R.L. (Eds.), *Stochastic Modeling and Geostatistics: Principles, Methods, and Case Studies*. AAPG Computer Applications in Geology.

- Pyrz, M.J., Deutsch, C.V., 2014. Geostatistical Reservoir Modeling. Oxford university press.
- Rezvandehy, M., Deutsch, C.V., 2018. Declustering experimental variograms by global estimation with fourth order moments. *Stoch. Environ. Res. Risk Assess.* 32 (1), 261–277.
- Schlumberger, 2014. Petrel Petrophysical Modeling Manual: Petrel E&P Software Platform 2014.
- Shepherd, M., 2009. Oil Field Production Geology: AAPG Memoir 91, vol. 91 AAPG.
- Sun, L., 2003. Sandstone-conglomerate bodies in Sha 3-4 members and hydrocarbon accumulation in northern slop of Dongying sag. *Acta Sedimentol. Sin.* 21 (2), 278–282.
- Wang, X., Hou, J., Liu, Y., Ji, L., Sun, J., 2017. Studying reservoir heterogeneity by analytic hierarchy process and fuzzy logic, case study of Es1x formation of the Wang guan tun oilfield, China. *J. Petrol. Sci. Eng.* 156, 858–867.
- Wang, X., Hou, J., Song, S., Wang, D., Gong, L., Ma, K., et al., 2018. Combining pressure-controlled porosimetry and rate-controlled porosimetry to investigate the fractal characteristics of full-range pores in tight oil reservoirs. *J. Petrol. Sci. Eng.* 171, 353–361.
- Xian, B., Lu, Z., She, Y., Wang, X., Wang, L., Huang, H., 2014. Sedimentary and reservoir characteristics of glutenite in Yan 18-Yong 921 area, steep slope of Dongying Sag. *Lithologic reservoirs* 26 (4), 28–36.
- Xu, Z., Zhang, B., Li, F., Cao, G., Liu, Y., 2018. Well logs decomposition using VMD in assisting the sequence stratigraphic analysis of a conglomerate reservoir. *Geophysics* 83 (4), 1–28.
- Zhang, L., Yang, W., 2012. Multi-provenance depositional model of paleo gully in north steep slope of dongying depression of upper Es₄ in paleogene. *J. Cent. S. Univ.* 43 (8), 3159–3165.
- Zhang, D., Feng, Y., Qiu, Y., Min, W., Guo, Y., Zhao, L., Xiang, L., 2004. Lower tertiary sequence stratigraphy study and the forecast of subtle reservoir in Dongying depression: sedimentologica Sinica. *Acta Sedimentol. Sin.* 22 (1), 67–72.